Precambrian Research 225 (2013) 218–229

Contents lists available at ScienceDirect

Precambrian Research

journal homepage: www.elsevier.com/locate/precamres

Trace and rare earth element geochemistry of black shale and kerogen in the early Cambrian Niutitang Formation in Guizhou province, South China: Constraints for redox environments and origin of metal enrichments

Dao-Hui Pi[a,b,c], Cong-Qiang Liu[b], Graham A. Shields-Zhou[d,e], Shao-Yong Jiang[a,*]

[a] State Key Laboratory for Mineral Deposits Research, Department of Earth Sciences, Nanjing University, Nanjing 210093, China
[b] Institute of Geochemistry, Chinese Academy of Sciences, Guiyang 550002, China
[c] Faculty of Earth Resources, China University of Geosciences, Wuhan 430074, China
[d] Department of Earth Sciences, University College London, Gower Street, London WC1E 6BT, UK
[e] State Key Laboratory for Palaeobiology and Stratigraphy, Nanjing Institute of Geology and Palaeontology, Chinese Academy of Sciences, Nanjing 210008, China

ARTICLE INFO

Article history:
Received 21 April 2011
Received in revised form 11 July 2011
Accepted 13 July 2011
Available online 4 August 2011

Keywords:
Redox-sensitive trace elements
Rare earth elements
Kerogen
Black shale
Redox conditions
Hydrothermal venting
Early Cambrian
South China

ABSTRACT

Early Cambrian black shales of South China not only host important sponge, arthropod and other soft-bodied fossils that have helped to trace early metazoan diversification, but also show extreme enrichments of a number of trace metals in particular Ni, Mo and V. In this study, we use a new approach by analyzing rare earth elements in kerogen extracted from the black shales, together with a number of redox-sensitive trace element compositions and total organic carbon (TOC) concentrations in an early Cambrian black shale sequence in Zunyi, Guizhou province, South China, to place better constraints on the oceanic redox conditions and the origin of the extreme metal enrichment.

Our data show significant negative Ce anomalies (Ce/Ce^* as low as 0.4) occurring in kerogen, which indicate an oxygenated surface environment of primary productivity in consistent with the concept that the organic matter is mainly derived from organisms in the euphotic zone. Mass balance calculation suggests that the kerogen-associated REE can dominate the measured black shale REE budget, while similarity between our measured REE patterns and those of similarly aged phosphorites indicates that the REE content of ancient phosphorites may have also derived initially from organic matter.

The redox-sensitive trace elements, such as U, V, Mo, and their ratios of U/Al, V/Al and Mo/Al in black shales show different correlation patterns with TOC contents. The upper black shales show a good metal/TOC correlation, but such a correlation is absent in the lower part. The lower black shales exhibit much higher metal enrichments compared to Black Sea sulphidic (euxinic) sediment. This is taken to indicate the presence of sulphidic bottom waters during the deposition of the lower black shales, including the Ni–Mo ore layer. In contrast, anoxic, non-sulphidic conditions occurred during the deposition of the upper black shales.

Taking all these geochemical data together, we suggest that the early Cambrian South China seaway was strongly stratified and stagnant, and that euxinic bottom water conditions may have led to enrichment of the redox-sensitive metals such as U, V and Mo in the lower black shales, and in one case the occurrence of a polymetallic Ni–Mo sulphide ore bed bearing an extraordinarily extreme metal enrichment, which, according to the Mo/TOC and Ni/TOC ratios and much other geochemical evidence, may have been additionally influenced by hydrothermal input of metals within the rift basin as suggested by a number of previous studies.

1. Introduction

The early Cambrian is characterized by a unique and abrupt increase in the abundance and diversity of fossils, an event also known as the 'Cambrian Explosion' (Brasier, 1992; Amthor et al., 2003). Changes in the ambient environment represent one possible explanation for this evolutionary diversification, but this is still a matter of debate (e.g., Brasier, 1992; Amthor et al., 2003; Scott et al., 2008; Wille et al., 2008). Marine sedimentary rocks of early Cambrian age are developed widely throughout South China (Zhu et al., 2004; Jiang et al., 2006). They record the oceanic/basinal environmental conditions during their formation and so provide a good

* Corresponding author.
E-mail address: shyjiang@nju.edu.cn (S.-Y. Jiang).

0301-9268/$ – see front matter © 2011 Elsevier B.V. All rights reserved.
doi:10.1016/j.precamres.2011.07.004

chance to explore the possible interactions between evolution and environment during the 'Cambrian Explosion'.

The 'Cambrian Explosion' in South China can be divided into three stages characterized by: (1) occurrence of small shelly fossils in the Zhongyicun phosphorites, (2) occurrence of the sponge and arthropod fossils in the Niutitang/Hetang black shales, and (3) occurrence of the trilobite and other metazoan fossils in the Yu'anshan grey/green shales (e.g., Shen et al., 2000; Steiner et al., 2001, 2007; Li et al., 2007; Weber et al., 2007; Zhou and Jiang, 2009). It is suggested that the depositional environment changed prior to the first stage of the Cambrian explosion in South China (e.g., Brasier et al., 1990; Shen et al., 1998, 2000; Shen and Schidlowski, 2000), with the spread of bottom water anoxia (Shields and Stille, 2001). The rapid diversification of small shelly invertebrates during this stage was, thus, ascribed to the upwelling of nutrient-rich waters (Shen et al., 2000). The sedimentary environment during the second stage has also been explored, and anoxia/euxinia in bottom waters have been suggested by many researchers based on the strong enrichments of redox-sensitive trace elements, high DOP values and a negative Mo isotopic excursion in the Niutitang black shales (e.g., Goldberg et al., 2007; Guo et al., 2007a; Lehmann et al., 2007; Jiang et al., 2007a, 2009; Wille et al., 2008; Zhou and Jiang, 2009).

The presence of abundant benthic animals such as sponges and arthropods, found apparently in situ, points to oxic or dysoxic living conditions beneath bottom waters in apparent contradiction to geochemical interpretations. In order to reconcile this conflict, Steiner et al. (2001) considered that these organisms were related to hydrothermal vents, while Zhou and Jiang (2009) thought that sponge growth was linked to occasional currents that brought free oxygen to the bottom water column. In addition, bottom water anoxia did not fit with some geochemical data. Firstly, significant Ce depletions were observed in the Niutitang black shales (Guo et al., 2007a) even though such conditions are generally thought to be characteristic of sediments deposited under oxic conditions (Shields and Stille, 2001). Because of this, Guo et al. (2007a) considered that the 'negative Ce anomalies' might derive primarily from biogenic silica from siliceous plankton that lived above a mid-water redox boundary. However, kerogen is another likely source of REE as we discuss below. Secondly, the Niutitang black shales host a polymetallic Ni–Mo sulphide ore layer which contains Ni and Mo up to 8.3% and 18%, respectively (Fan, 1983; Coveney et al., 1992). Mao et al. (2002) and Lehmann et al. (2007) presumed that the sulphide layer formed through synsedimentary metal precipitation directly from seawater under strongly reducing conditions, but no analogy is known from modern stagnant basins or from ancient black shales (Steiner et al., 2001; Coveney, 2003). Based on Os isotopic compositions and other geological and geochemical data, Jiang et al. (2004, 2006, 2007a,b) and others (e.g., Lott et al., 1999; Steiner et al., 2001; Pan et al., 2004; Yang et al., 2004; Orberger et al., 2007) have ascribed these extreme metal enrichments to submarine hydrothermal activity. Thirdly, Lehmann et al. (2007), based on the Mo isotopic compositions in the Niutitang Formation, suggested that anoxic depositional environments were more prevalent in the Early Cambrian oceans than today; while Scott et al. (2008) inferred that deep ocean water was well oxygenated by 551 Ma from Mo/TOC ratios in sulphidic black shales.

Trace elements such as U, V and Mo are sensitive to redox changes in the water column and are highly enriched in reducing sediments, potentially making them robust proxies for paleoredox conditions (Tribovillard et al., 2006). In previous studies, the trace elemental concentrations and ratios, such as U, Mo, V, U/Th and V/(V + Ni), were used to constrain redox conditions in the early Cambrian ocean (e.g., Yang et al., 2004; Jiang et al., 2006; Guo et al., 2007a), but no attention was paid to correlations between trace element and organic carbon contents. In fact, the trace element–total organic carbon (TOC) correlations are more effective in discerning redox grade (Tribovillard et al., 2006) and so are explored here in more detail.

In this paper, we applied a new approach by analyzing the rare earth element contents in kerogen from the black shales, in combination with redox-sensitive trace elements and organic carbon concentrations (TOC) on an early Cambrian black shale sequence in Zunyi, Guizhou province, South China, in an attempt to place a better constraint on: (1) the sedimentary redox conditions at the time of black shale deposition, (2) the origin of REE in black shales, and (3) the origin of the enigmatic polymetallic Ni–Mo ore layer in South China.

2. Geological setting and studied section

During early Cambrian times, the Yangtze Block occurred three sedimentary facies from northwest to southeast: (1) carbonate platform, (2) transitional belt and (3) deep-water basin (Fig. 1). The transitional belt is characterized by protected basins which were former back-arc basins (Steiner et al., 2001). The protected basins are believed to have faced open oceans to the southeast (McKerrow et al., 1992) and to have enjoyed continuous communication with oxic seawater in the surface oxic layer (Lehmann et al., 2007). Transitional belt successions are characterized by a transgressive black shale sequence (Zhujiajing/Niutitang/Hetang Formation) with abundant fossils, such as sponge and arthropod body fossils (Steiner et al., 2001; Goldberg et al., 2007; Zhou and Jiang, 2009). In the deep-water basin occurred an organic-rich black chert sequence (Liuchapo Formation), in which no fossil has hitherto been reported (Li et al., 2007).

The investigated Zhongnancun section in this study is located ca. 15 km west of Zunyi, Guizhou (N 27°41′24.6″, E 106°40′45.2″) and lies paleogeographically in the protected basin facies (Fig. 1). Most units of this section were described by Steiner et al. (2001). According to our lithostratigraphic analysis, the profile can be divided into ten units (Fig. 2):

Unit 1: brownish to black siliceous phosphorite (65 cm in thickness), unconformably overlying dolomite of the Neoproterozoic Dengying Formation with an iron–manganese oxide-rich weathering crust (20 cm in thickness) between them. The Precambrian–Cambrian boundary is usually placed at the bottom of this unit (Steiner et al., 2001). An equivalent unit was found to contain small shelly fossils, and can reach several meters in thickness at Zhijin, where it is mined for phosphate ore.

Unit 2: grey to black pyrite-rich claystone (27 cm in thickness). The change in color is due to its elevated organic concentration. Pyrite crystal cubes with sizes of ~3 mm are found, commonly enveloped by green glauconite (~5 mm in diameter) and distributed parallel to bedding. The thickness of this unit is highly variable.

Unit 3: grey to black tuff (or K-bentonite) intercalated with black chert (28 cm in thickness). The dark color of the tuff is caused by abundant organic matter. The grey tuff is very cracked and loose, and is very sticky when wet. Many euhedral zircons (20–120 μm in length) were separated from it and provided good age constraints (Jiang et al., 2009). In addition, pyritoid pyrites were also abundant. This unit is also highly variable in thickness.

Unit 4: black chert intercalated with black shale (1.72 m in thickness). The black cherts are rich in organic matter up to 15% (Table 1), and sometimes contain minor sulphides; while the black shales contain lots of phosphatic nodules (1–5 cm in diameter), organic debris (<5 mm) and abundant hydromicas.

Unit 5: deep black Vanadium ore layer (3 cm in thickness). Since this unit looks like black shale, it is easily overlooked. However, some features can be used to identify this unit in the field, such

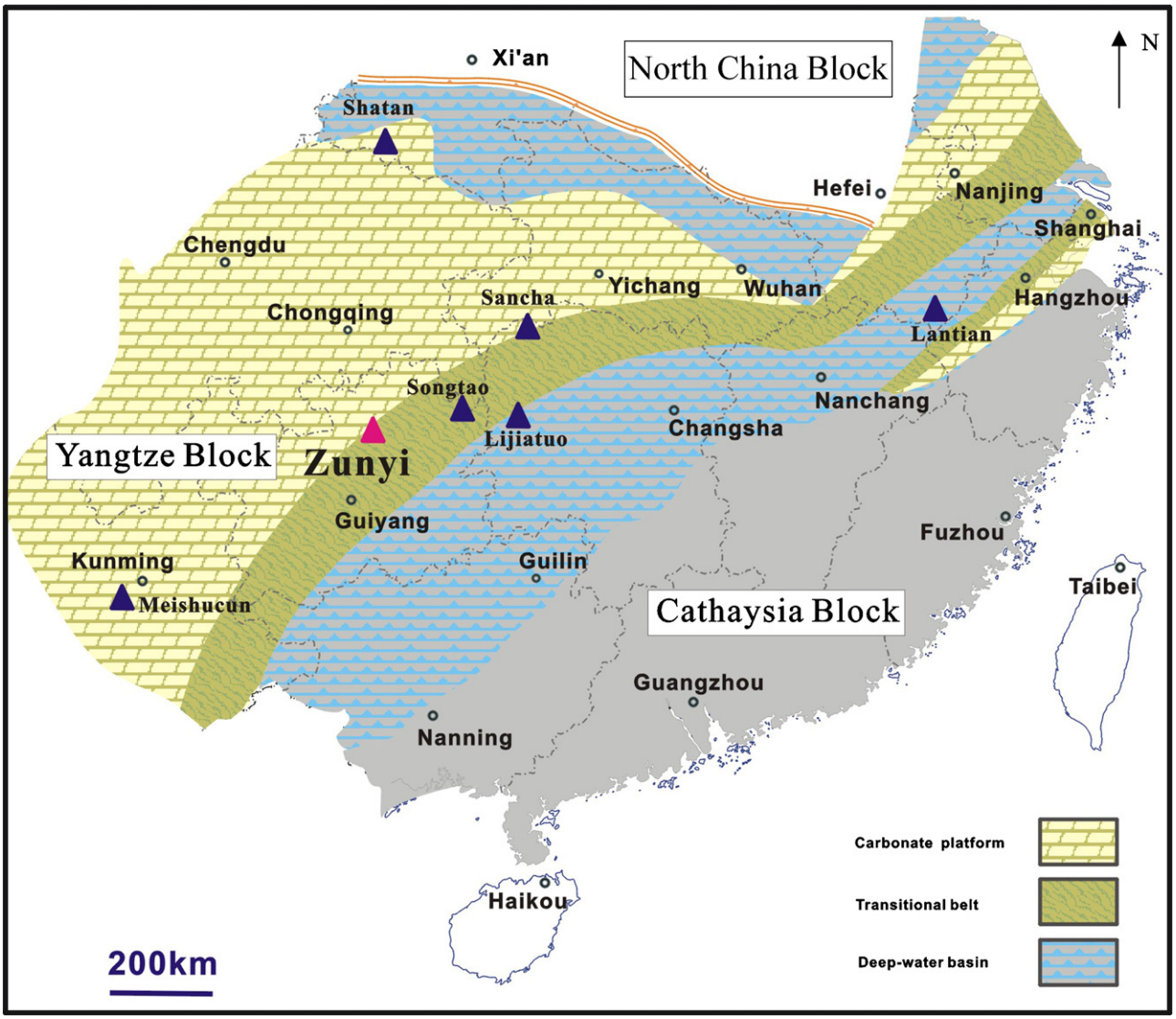

Fig. 1. Map showing the locations and depositional environments of the investigated section on Yangtze Platform, South China (modified from Jiang et al., 2007a). Red triangle is our studied section; blue ones are other sections studied previously. (For interpretation of the references to colour in this figure legend, the reader is referred to the web version of the article.)

as its darker color, coarser surface, no macroscopic hydromica, and no laminae. The V concentration can be up to 6.4% (Table 1). The grade of the Vanadium ore is commonly ~1 wt% in places and has been mined by local miners in Guizhou, Hunan, Jiangxi, and Hubei provinces. Several studies have shown that the Vanadium is mainly incorporated into the clay minerals such as illite, some are also associated with organic matter (Zhang et al., 1987; Yang, 2008).

Unit 6: black shale (2.96 m in thickness) containing organic debris, phosphatic nodules and minor sulphides.

Unit 7: Ni–Mo sulphide ore layer with underlying limestone concretions (15 cm in thickness). Due to exposure, the ore has been weathered but sulphide minerals are still present.

Unit 8: black shale with abundant fossils (5.38 m in thickness). This unit contains lots of fossils, such as sponge spicules and bivalved arthropods with few phosphatic nodules.

Unit 9: black shale (10.35 m in thickness) with rare fossils.

Unit 10: silty black shale (10.3 m in thickness) without nodules. The overlying stratum of this unit is green shale which was reported to contain abundant eodiscid trilobites (Steiner et al., 2001).

Lithological correlation between the Zhongnancun section and the Meishucun section, Yunnan, a former candidate of the chronostratigraphic *Global Stratigraphic Section and Point* (GSSP) for the Precambrian–Cambrian boundary, showed that the Unit 1 was equivalent to the Zhongyicun Member of the Zhujiaqing Formation, and that Unit 4 was equivalent to the base of the Shiyantou Formation (Zhu et al., 2004). Correlation from occurrences of fossils and polymetallic Ni–Mo sulphide ore indicated that Units 7–8 were of 'late Tommotian' age (Steiner et al., 2001). The absolute age of the polymetallic Ni–Mo sulphide ore (Unit 7) was initially dated using Re–Os method by Horan et al. (1994) with an imprecise age of 560 ± 50 Ma; then Mao et al. (2002) and Li et al. (2003) reported more precise Re–Os isochron ages of 541 ± 16 Ma and 542 ± 11 Ma for the Ni–Mo sulphide ores, respectively. These data were recalculated to yield an age of 537 ± 10 Ma (Jiang et al., 2004). The age of the tuff (Unit 3) was also dated at 532.3 ± 0.7 Ma (1 SE) using zircon SHRIMP U–Pb dating method by Jiang et al. (2009). The latter age is identical within error to that of the tuff (Bed 5) in Zhongyicun Member in the Meishucun section (534.9 ± 1.9 Ma, recalculated by us with data from Sawaki et al., 2008 after common Pb correction). A similar age of

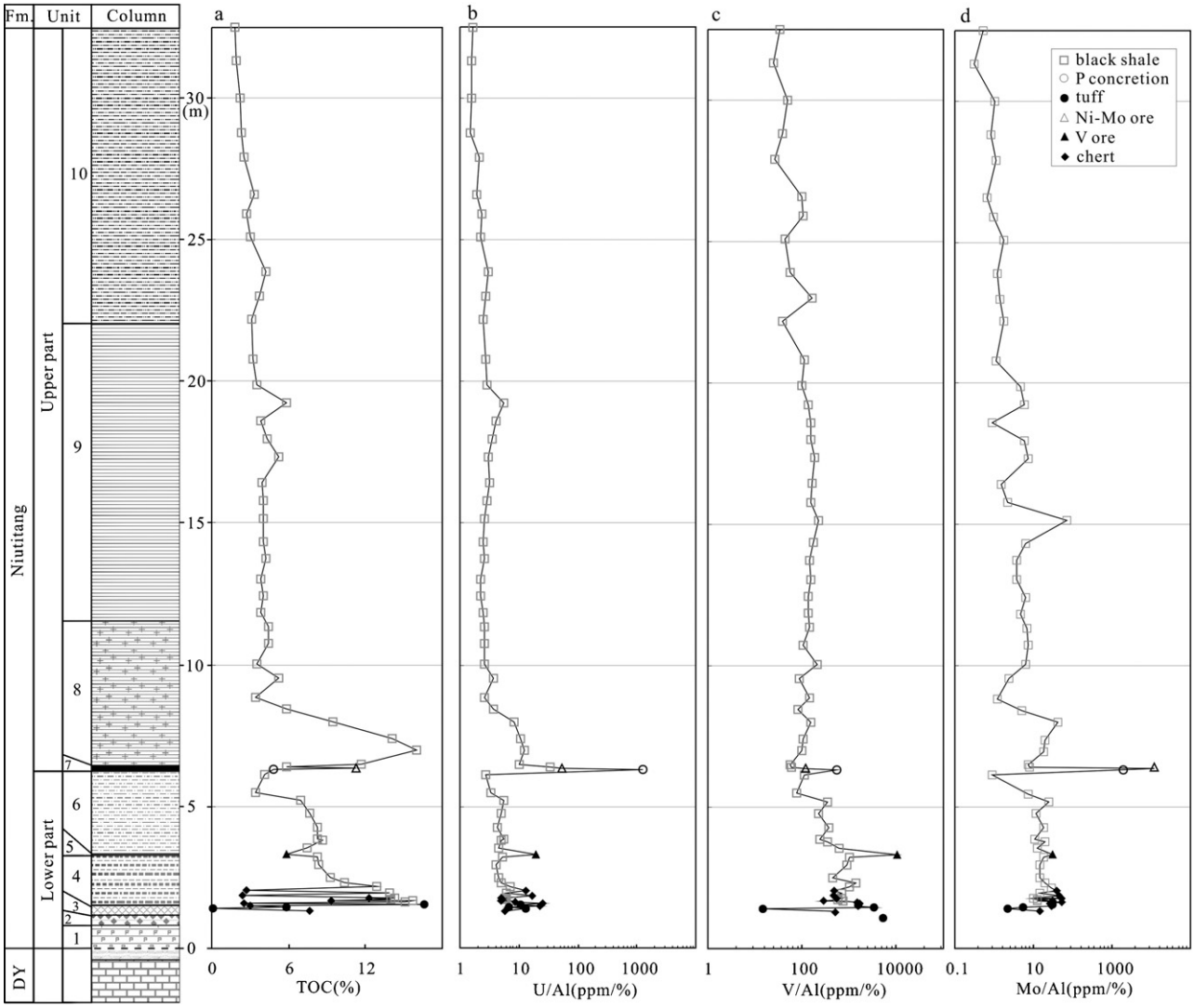

Fig. 2. Stratigraphic column and variation trends of (a) TOC, (b) U/Al, (c) V/Al, and (d) Mo/Al for sedimentary rocks in the Zhongnancun section in Zunyi, South China. DY: Dengying formation (Ediacaran).

Table 1
REE contents in organic matter of early Cambrian Niutitang Formation sedimentary rocks from the Zhongnancun section in Zunyi, South China (ppm).

Sample	La	Ce	Pr	Nd	Sm	Eu	Gd	Tb	Dy	Ho	Er	Tm	Yb	Lu	Y	Ce/Ce*
ZN04-20	8.29	10.8	1.46	4.79	0.912	0.120	0.991	0.162	0.831	0.153	0.394	0.054	0.235	0.026	3.14	0.71
ZN04-22	82.6	114	18.3	79.4	25.2	4.30	31.7	4.10	20.4	3.35	6.89	0.690	2.77	0.303	61.1	0.64
ZN04-23-2	167	208	30.0	102	14.2	2.04	13.3	1.38	5.65	0.978	2.23	0.248	1.17	0.157	31.0	0.67
ZN04-24	3.45	3.95	0.676	2.32	0.345	0.053	0.344	0.039	0.182	0.036	0.094	0.011	0.059	0.005	1.31	0.60
ZN04-25-1	28.3	22.9	3.86	14.7	2.93	0.516	4.28	0.566	3.26	0.709	1.80	0.211	0.963	0.130	27.1	0.45
ZN04-25-3	8.11	6.11	1.12	5.19	1.41	0.296	2.23	0.309	1.91	0.423	1.13	0.134	0.586	0.082	16.5	0.40
ZN04-25-5	14.1	10.3	1.83	8.13	2.06	0.417	3.18	0.415	2.44	0.524	1.33	0.143	0.630	0.084	19.9	0.40
ZN04-27	40.9	40.9	6.87	25.5	4.84	0.954	6.39	0.817	4.41	0.839	2.10	0.233	1.20	0.146	32.1	0.53
ZN04-29	22.0	17.4	3.24	12.6	2.58	0.557	3.88	0.491	2.99	0.663	1.71	0.207	1.00	0.145	26.8	0.43
ZN04-30	27.1	25.3	4.61	17.0	2.85	0.622	3.90	0.500	2.64	0.566	1.47	0.175	0.807	0.116	20.2	0.50
ZN04-31	28.6	33.4	5.72	22.9	4.68	1.00	6.31	0.791	4.40	0.872	2.15	0.250	1.13	0.154	26.9	0.58
ZN04-32	31.1	49.8	7.86	30.6	4.88	0.956	5.51	0.676	3.29	0.611	1.48	0.168	0.883	0.105	18.7	0.74
ZN04-34	87.8	107	15.5	52.6	6.51	1.43	8.72	1.05	5.74	1.28	3.30	0.389	1.89	0.276	53.9	0.66
ZN04-35	28.4	48.4	7.59	31.4	7.07	1.48	8.47	1.10	5.70	1.05	2.54	0.312	1.52	0.193	27.9	0.76
ZN04-36	31.5	56.7	8.87	36.6	5.75	0.888	4.11	0.421	1.42	0.211	0.473	0.057	0.333	0.041	5.93	0.78
ZN04-37	50.7	100	18.3	88.7	16.2	2.66	12.0	1.18	4.01	0.577	1.16	0.124	0.592	0.076	14.1	0.72
ZN04-56	41.6	59.6	7.30	26.1	4.60	0.959	4.34	0.502	2.08	0.348	0.785	0.082	0.405	0.049	8.30	0.76
ZN04-57	27.7	45.2	5.55	18.4	2.68	0.513	2.39	0.262	1.10	0.210	0.587	0.074	0.391	0.054	7.41	0.85
ZN04-58	27.6	41.0	5.17	17.4	2.60	0.490	2.12	0.238	1.05	0.217	0.585	0.080	0.461	0.056	7.92	0.79
ZN04-59	10.8	16.1	1.76	6.49	1.40	0.329	1.32	0.145	0.712	0.133	0.382	0.049	0.281	0.038	4.38	0.80
ZN04-60	16.4	29.8	3.59	12.5	1.95	0.375	1.31	0.169	0.710	0.137	0.388	0.056	0.309	0.044	4.17	0.92
ZN04-70	27.2	46.3	5.68	22.3	6.82	1.55	7.33	1.06	5.69	1.07	2.92	0.395	2.16	0.358	28.4	0.84

$Ce/Ce^* = 3Ce_N/(2La_N + Nd_N)$, where N referred to normalization of concentrations against the shale standard PAAS (McLennan, 1989).

535.2 ± 1.7 Ma for the Bed 5 was also reported by Zhu et al. (2009) using the Cameca 1280 SIMS U–Pb dating method. These new age data indicate a good correlation of these two tuff beds with each other.

3. Samples and analytical methods

A total of 66 samples were collected from the Zhongnancun section. The samples included: one phosphatic concretion (ZN04-53), one V ore (ZN04-34), three tuffs (ZN04-21, ZN04-22 and ZN04-23-2), eight cherts (ZN04-20, ZN04-23-1, ZN04-23-3, ZN04-24, ZN04-25-2, ZN04-25-4, ZN04-26 and ZN04-28), and 53 black shales. In addition, one Ni–Mo sulphide ore (ZN04-54) sample was taken from a nearby underground mine adit.

Trace elements U, V, Mo, Ni, Sc, Zr, Th and the major element Al were analyzed in this study. Because organic matter cannot be digested completely by microwave oven, we applied a more effective digestion procedure as follows: Firstly, ~1.0 g sample powder was weighed into a porcelain crucible, and was combusted in a muffle oven at 800 °C for 2 h, and weighed again after the crucible cooled. The mass lost on ignition was recorded and used for later correction. Then, ~100 mg of the ashed sample was weighed into a PTFE microwave digest vessel, followed by addition of 4 ml HNO_3, 1 ml HF and 1 ml $HClO_4$. The mixture was allowed to react for a couple of hours and then subjected to Microwave-assisted heating. After cooling down, the resulting solution was transferred quantitatively into a 100 ml PTFE beaker, and the solution was heated on a hotplate until dry. Subsequently, another 1 ml $HClO_4$ was added and was heated again till dry to drive out HF. Finally, the material was redissolved in 20% HNO_3 and diluted to 50 ml with double distilled water. The obtained sample solution was diluted a further 5 fold for ICP–MS analysis (Varian Single Collector Quadrupole 820). During analysis, we used In as an internal standard and its concentration in sample solution was 80 ppb. A commercially available multi-element standard was used to calibrate the instrument externally, and a certified reference material SDO-1 was used to validate this measurement and used for quality control purposes. Results were corrected to the weight of bulk rock, and analytical precision for trace element concentration was better than 5%.

REE and Y contents in organic matter (kerogen) were analyzed for 22 samples. Firstly, about 1 g of sample powder was leached with 10% HNO_3 to remove carbonate, phosphate and sulphides. Then, it was dried at 60 °C and weighed before being combusted at 550 °C. Subsequently, this ashed sample was leached with 10% HNO_3 to extract REE. The obtained solution was treated and measured according to the procedure described above, while the residual was dried and weighed again. Data were reported with respect to the weight of organic matter which was calculated from the difference in weight measurements between pre-combustion and post-HNO_3 leaching. Analytical precision was better than 5%. Cerium anomaly ($Ce/Ce^* = 3Ce_N/(2La_N + Nd_N)$), Eu anomaly ($Eu/Eu^* = Eu_N/(Sm_N \times Gd_N)^{1/2}$), Pr anomaly ($Pr/Pr^* = 2Pr_N/(Ce_N + Nd_N)$), and Y anomaly ($Y/Y^* = 2Y_N/(Dy_N + Ho_N)$) were calculated according to Shields and Stille (2001), where N refers to normalization of concentrations against the shale standard PAAS (McLennan, 1989).

Total organic carbon (TOC) abundances of all samples were measured by Elemental Analyzer (Vario MAX CNS), after removal of carbonate with 10% HCl. Results were corrected to the weight of bulk rocks, and analytical precision was better than 0.1%.

All of the above analyses were conducted at the Advanced Analytical Centre of James Cook University, Australia.

4. Results

Rare earth element (REE) and Y abundances of kerogen in the early Cambrian Niutitang sedimentary rocks are presented in Table 1. Total concentrations of REE vary from 11.6 to 548 ppm with the lowest value in a chert (ZN04-24) and the highest value in a tuff (ZN04-23-2). The Ce/Ce* values vary between 0.40 and 0.92, while the Eu/Eu* values vary between 0.59 and 1.14.

Trace element (U, V, Mo, Ni, Sc, Zr and Th), and major element (Al) abundances in the early Cambrian Niutitang sedimentary rocks are listed in Table 2. The redox-sensitive trace elements U, V, Mo, and Ni show a variation from 4.1 to 746 ppm, 111 to 63,900 ppm, 3.3 to 33,900 ppm, and 21 to 44,300 ppm, respectively. All these elemental abundances display a decreasing trend up-section (Fig. 2b–d). They show variable enrichment factors (1~1000 times) compared to the average upper continental crust (Taylor and McLennan, 1985). Scandium, Zr, Th, and Al abundances vary according to lithology with lower values in chert and phosphatic concretion and higher values in tuff.

TOC abundances are also listed in Table 2. TOC abundances vary from 0.09% to 16.6%. The TOC abundances display obvious stratigraphic variations: an obvious decreasing trend up-section and a remarkable peak immediately above the polymetallic Ni–Mo sulphide ore (Fig. 2a). The TOC peak corresponds to the appearance of sponge spicules in section.

5. Discussion

5.1. REE pattern and Ce anomaly of organic matters in black shale

The bulk REE concentrations in sedimentary rocks reflect contributions from both authigenic and detrital components, while it is only the REE in authigenic precipitates, such as carbonate, phosphate, and probably chert that originate from seawater (Shields and Stille, 2001; Feng et al., 2004; Jiang et al., 2007b). When the contribution of REE from authigenic components is insignificant, the bulk shale-normalised REE will display a flat pattern which is typical for terrestrial detritus. Organic matter in sedimentary rocks derives mainly from phytoplankton and, to a lesser extent, zooplankton and bacteria (Lewan, 1986), and thus also can be regarded as a special kind of authigenic component. Unlike carbonate, the organic matter generally contains high amounts of REE, for example, Mossman et al. (1993) reported that Proterozoic stratiform kerogen and globular bitumen may contain up to thousands ppm REE, and Felitsyn et al. (1998) found macroscopic organic fossils of the latest Neoproterozoic to earliest Cambrian can contain up to 200 ppm REE. Therefore, the REE in kerogen from sedimentary rocks may provide a new window to explore oceanic redox conditions.

In the present study, the REE patterns of kerogen in Niutitang Formation black shales can be divided into four groups (Fig. 3): Group I, slight enrichments of LREE with moderate negative Ce anomalies (Fig. 3a); Group II, moderate enrichments of MREE with moderate to strong negative Ce anomalies (Fig. 3b); Group III, strong depletions of HREE with weak or no negative Ce anomalies (Fig. 3c), and Group IV, mild enrichments of HREE with almost no significant Ce anomaly (Fig. 3d). Obviously, none of them is fully consistent with the seawater-like REE pattern which shows a progressive enrichment towards the heavier REE and a relative depletion of Ce with respect to its REE neighbors La and Pr, or Nd (Fig. 3d). However, the significant negative Ce anomalies are similar to that of modern seawater.

The negative Ce anomaly is related to the oxidation of Ce(III) to Ce(IV) (Sholkovitz et al., 1994), and thus can trace redox conditions (Elderfield and Greaves, 1982; Wright et al., 1987), when signals are not obliterated by post-depositional diagenetic REE exchange

Table 2
Trace elements and total organic carbon (TOC) concentrations for the early Cambrian Niutitang Formation sedimentary rocks from the Zhongnancun section in Zunyi, South China.

Sample	Lithology	Unit	Height[a] (cm)	TOC (%)	Al (%)	Sc (%)	Zr (ppm)	Th (ppm)	U (ppm)	V (ppm)	Mo (ppm)	Ni (ppm)	Mo/TOC (ppm/%)
ZN04-90	Silty black shale	10	3249	1.78	10.43	20.3	165	15.2	17.1	362	5.64	49.5	3.2
ZN04-89	Silty black shale	10	3129	1.94	10.24	20.8	186	14.3	15.8	255	3.29	47.2	1.7
ZN04-88	Silty black shale	10	2999	2.20	10.22	21.4	176	15.2	15.9	492	10.8	73.5	4.9
ZN04-87	Silty black shale	10	2879	2.29	10.58	20.8	177	14.6	15.7	414	8.47	56.3	3.7
ZN04-86	Silty black shale	10	2789	2.53	9.74	21.3	196	14.0	21.0	263	11.3	25.8	4.5
ZN04-85	Silty black shale	10	2659	3.36	9.71	20.3	172	14.0	19.1	953	6.19	83.0	1.8
ZN04-84	Silty black shale	10	2589	2.69	9.56	19.9	174	14.1	22.2	993	9.29	76.9	3.5
ZN04-83	Silty black shale	10	2509	3.02	10.43	20.3	165	13.8	23.0	461	17.9	86.5	5.9
ZN04-82	Silty black shale	10	2389	4.19	8.70	20.1	174	14.9	26.4	498	10.2	41.9	2.4
ZN04-81	Silty black shale	10	2299	3.73	8.83	20.0	166	14.7	24.3	1412	12.8	47.1	3.4
ZN04-80	Black shale	9	2219	3.08	9.49	21.6	185	16.7	23.6	354	16.4	31.8	5.3
ZN04-79	Black shale	9	2079	3.19	8.10	19.0	159	13.1	22.3	929	8.96	81.5	2.8
ZN04-78	Black shale	9	1989	3.56	8.08	19.3	164	13.8	22.9	788	39.1	153	11.0
ZN04-77	Black shale	9	1924	5.82	7.48	19.1	171	14.6	41.5	982	44.3	146	7.6
ZN04-76	Black shale	9	1859	3.82	7.94	18.8	169	13.8	32.1	1207	7.25	66.9	1.9
ZN04-75	Black shale	9	1799	4.33	7.37	18.7	163	11.7	26.3	1124	44.1	103	10.2
ZN04-74	Black shale	9	1734	5.22	8.07	17.5	126	13.6	24.3	1487	61.7	84.9	11.8
ZN04-73	Black shale	9	1644	3.89	8.63	20.9	153	15.6	27.2	1399	12.7	56.8	3.3
ZN04-72	Black shale	9	1579	3.97	8.72	19.3	138	14.7	24.8	1347	19.4	70.3	4.9
ZN04-71	Black shale	9	1514	3.98	8.99	19.7	141	16.3	23.0	1951	622	95.7	156
ZN04-70	Black shale	9	1434	4.01	8.19	18.4	128	14.0	20.1	1463	50.5	75.0	12.6
ZN04-69	Black shale	9	1374	4.25	8.88	20.4	149	16.6	23.4	1275	33.3	80.6	7.8
ZN04-68	Black shale	9	1304	3.82	8.76	18.4	138	15.9	19.5	1317	32.5	106	8.5
ZN04-67	Black shale	9	1244	4.07	8.66	18.0	140	15.5	19.8	1184	53.2	84.3	13.1
ZN04-66	Black shale	8	1184	3.82	8.96	18.3	140	16.4	21.6	1246	41.0	68.4	10.7
ZN04-65	Black shale	8	1134	4.40	8.33	19.5	137	15.3	22.2	1204	57.0	76.8	13.0
ZN04-64	Black shale	8	1074	4.43	8.43	19.9	147	15.0	22.1	869	60.7	80.1	13.7
ZN04-63	Black shale	8	1004	3.52	8.43	16.2	135	14.5	21.5	1793	52.8	100	15.0
ZN04-62	Black shale	8	954	5.27	8.34	20.1	145	15.5	30.6	714	20.3	77.8	3.8
ZN04-61	Black shale	8	884	3.44	9.36	22.2	134	19.5	24.2	1353	11.3	107	3.3
ZN04-60	Black shale	8	844	5.83	7.18	13.8	145	10.3	26.5	590	37.1	54.7	6.4
ZN04-59	Black shale	8	799	9.49	6.11	9.33	138	13.3	50.7	967	252	112	26.5
ZN04-58	Black shale	8	739	14.1	6.13	10.2	123	12.6	64.1	637	122	138	8.6
ZN04-57	Black shale	8	698	16.0	5.29	9.92	120	13.7	66.5	536	97.7	132	6.1
ZN04-56	Black shale	8	651	11.7	7.03	13.8	116	13.2	72.8	400	53.4	135	4.6
ZN04-55	Black shale	7	641	5.87	7.17	33.1	112	14.7	245	430	57.0	204.5	9.7
ZN04-54	Ni–Mo sulphide ore	7	637	11.1	2.01	5.00	50.0	4.20	180	612	48,350	41,700	3001
ZN04-53	Phosphatic concretion	7	632	4.87	0.59	2.07	0.657	0.159	746	315	1163	215	239
ZN04-52	Black shale	6	613	4.12	10.09	17.7	119	17.9	27.3	1134	9.20	213	2.2
ZN04-51	Black shale	6	548	3.42	7.29	13.0	99.0	13.8	24.6	545	54.2	188	15.8
ZN04-50	Black shale	6	520	6.92	4.77	10.0	101	11.9	26.0	1707	120	51.7	17.3
ZN04-39	Black shale	6	478	7.63	6.78	13.7	110	12.5	34.8	1557	76.6	62.3	10.0
ZN04-38	Black shale	6	427	8.29	6.32	12.0	102	9.80	26.7	2314	113	73.3	13.6
ZN04-37	Black shale	6	387	8.22	6.47	11.7	91.9	10.7	35.8	1581	71.4	98.9	8.7
ZN04-36	Black shale	6	379	8.66	6.87	9.21	83.8	6.22	33.7	2350	133	91.1	15.4
ZN04-35	Black shale	6	355	7.45	6.24	10.9	76.2	9.70	28.5	3714	77.7	200	10.4
ZN04-34	V ore	5	333	5.83	6.05	9.98	62.2	5.76	115	63,904	194	117	33.3
ZN04-33	Black shale	4	323	8.21	6.15	11.4	85.4	10.1	32.0	6266	109	183	13.2
ZN04-32	Black shale	4	297	8.36	5.60	10.7	73.0	9.70	22.9	5072	82.2	145	9.8
ZN04-31	Black shale	4	250	9.27	5.12	8.82	68.7	8.73	23.8	2351	74.1	179	8.0
ZN04-30	Black shale	4	230	10.3	4.55	8.01	73.5	8.11	22.9	6377	87.4	191	8.5
ZN04-29	Black shale	4	216	12.8	4.34	8.44	79.6	7.83	30.2	4359	121	172	9.4
ZN04-28	Chert	4	206	2.72	0.40	0.627	1.25	0.048	5.39	198	15.6	28.3	5.8
ZN04-27	Black shale	4	195	13.9	5.92	10.4	115	10.4	36.1	4061	83.1	176	6.0
ZN04-26	Chert	4	185	2.41	0.24	0.462	0.918	0.048	4.10	111	10.9	21.0	4.5
ZN04-25-5	Black shale	4	178	14.3	5.14	9.59	105	10.2	30.2	3491	51.1	87.7	3.6
ZN04-25-4	Chert	4	176	12.3	1.21	2.05	16.6	0.899	6.02	660	64.9	58.8	5.3
ZN04-25-3	Black shale	4	172	14.0	5.41	9.96	98.8	9.72	33.3	3112	67.2	105	4.8
ZN04-25-2	Chert	4	170	9.34	1.74	2.78	26.2	1.76	8.87	497	55.9	43.4	6.0
ZN04-25-1	Black shale	4	168	15.7	5.50	10.5	113	10.2	40.4	4017	68.5	110	4.4
ZN04-24	Chert	4	163	15.1	0.54	0.683	5.04	0.272	4.67	780	28.6	71.1	1.9
ZN04-23-3	Chert	3	157	2.54	0.19	0.256	1.20	0.048	4.84	323	5.21	24.2	2.1
ZN04-23-2	Tuff	3	154	16.6	8.46	8.90	132	10.1	91.1	13,091	256	199	15.4
ZN04-23-1	Chert	3	150	3.03	0.21	0.245	3.41	0.048	4.60	315	6.00	30.6	2.0
ZN04-22	Tuff	3	145	5.86	10.16	5.27	224	10.6	67.5	34,788	54.7	87.0	9.3
ZN04-21	Tuff	3	139	0.09	13.35	3.39	389	37.5	171	194	30.4	67.2	343
ZN04-20	Chert	3	133	7.65	0.86	1.05	28.9	0.639	4.93	423	12.3	44.0	1.6
Black Sea[b]	Euxinic sediment				4.88				16	141	21		

[a] Above the Ediacaran–Cambrian boundary (0 m).
[b] Data from Calvert and Pedersen (1993).

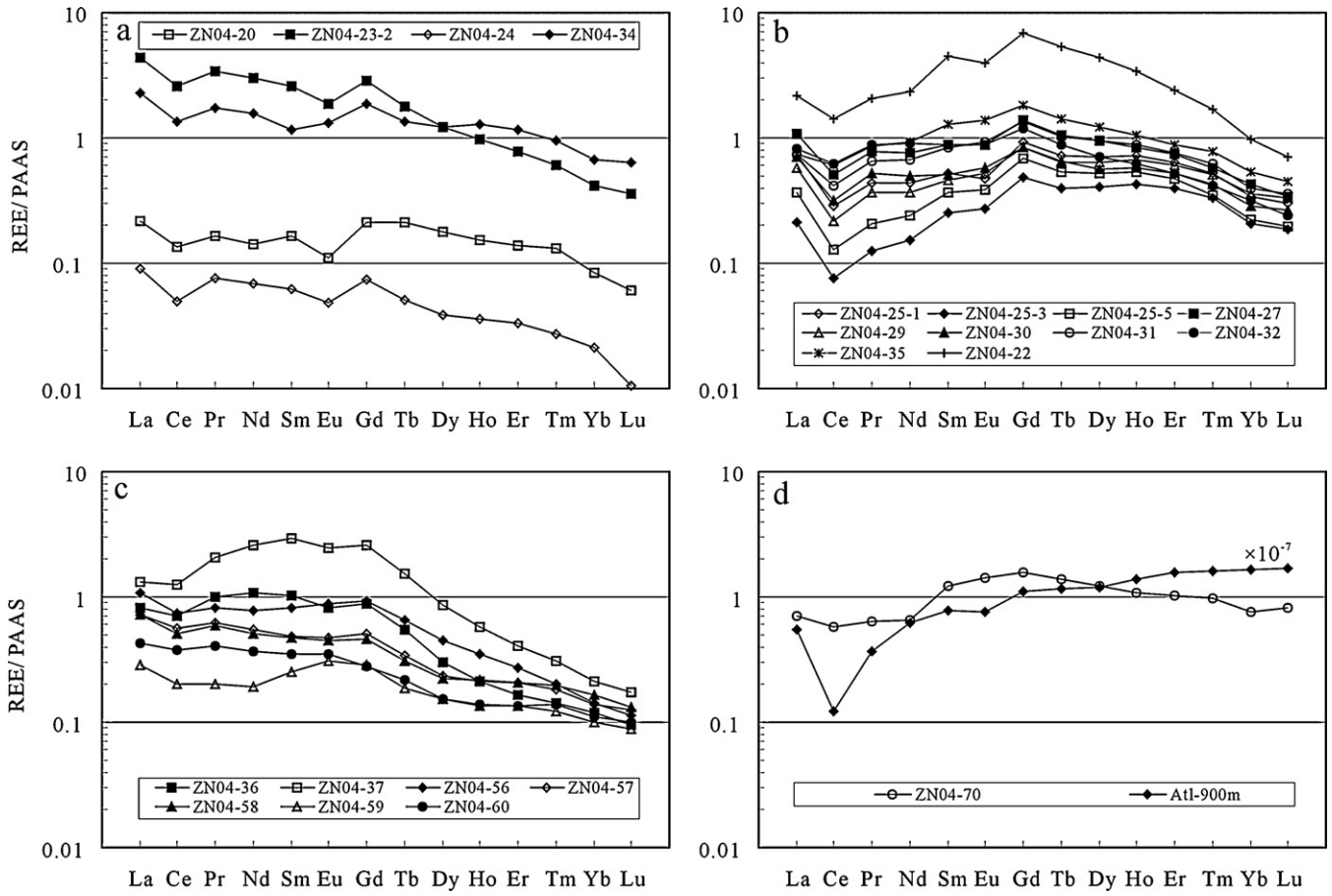

Fig. 3. PAAS shale-normalized REE distribution patterns of organic matter in sedimentary rocks from the Zhongnancun section in Zunyi, South China. Seawater REE pattern is defined by a water sample at 900 m depth in North Atlantic (Elderfield and Greaves, 1982).

(German and Elderfield, 1990; Shields and Stille, 2001; Felitsyn and Morad, 2002). In this study, the Ce anomalies correlate well with the Eu anomalies (Fig. 4a) but not with the bulk REE concentrations (Fig. 4b), indicating that the REE scavenging after deposition was weak. In addition, the plot of Ce anomalies against Pr anomalies (Fig. 4c) demonstrates that the negative Ce anomalies are genuine, instead of being exaggerated by enrichments of La (Shields and Stille, 2001). Therefore, the organic matter still retains primary Ce anomalies. The negative Ce anomalies (0.4–0.9) point to oxic conditions which are consistent with the concept that the organic matter is mainly derived from organisms in the euphotic zone (Kříbek et al., 2007), and imply that the carbon isotopic composition of kerogen in this study reflects surface DIC source.

In previous studies, REE investigations were always carried out on bulk rocks, and weak to moderate negative Ce anomalies (from 0.7 to 0.9) were observed in some black shales (e.g., Guo et al., 2007b; Lehmann et al., 2007). According to our study, these negative Ce anomalies are most probably derived from organic matter input. An illustration of how Ce anomalies in bulk rocks vary with REE contributions and primary Ce anomalies of organic matter (Fig. 5) shows that the negative Ce anomalies from 0.7 to 0.9 in bulk rocks correspond to 15–60% of bulk REE contributed by organic matter with Ce/Ce* values of 0.3–0.5. Although we did not conduct REE analyses on the bulk rocks in this study, a high proportion of REE supplied by organic matter is expected as the black shales are very rich in organic matter (up to 16% in TOC content in this study) and the organic matter is rich in REE (up to 500 ppm in this study).

Previous studies have shown that Early Cambrian phosphorites are generally characterized by 'old phosphorite' REE patterns, which are MREE enriched and HREE depleted (Shields and Stille, 2001). The differences from seawater patterns were ascribed to post-depositional REE exchange with non-detrital components and non-quantitative uptake of REE from host sediments during early diagenesis (Shields and Webb, 2004). Similarity between these patterns and the organic matter patterns suggests that organic matter may be the source of much REE enrichment in authigenic phosphorites (Felitsyn et al., 1998), since organic matter after decay would release REE to the commonly reducing pore fluid and then REE was re-incorporated by phosphate during early diagenetic scavenging.

5.2. Trace element geochemistry of bulk black shales

Trace element concentrations in bulk black shales are mixtures of both detrital and authigenic components, but it is only the concentrations of authigenic components that vary in response to redox changes in the water column. To estimate the authigenic enrichment of a given element, a customary way is to normalize it to aluminum (Al), which is commonly overwhelmingly of detrital origin and usually immobile during diagenesis (Algeo and Maynard, 2004). However, the enrichment can be overestimated or underestimated when Al originates from other relatively Al-rich or poor sources (Kryc et al., 2003). To address this problem, an easy way to check whether Al comes from a common siliclastic flux is to plot Al versus Sc, Th or Zr, which are also overwhelmingly of detrital origin. If good positive correlations are observed, it can be inferred that Al comes from a common siliclastic flux. In this study, the black shales exhibit good positive correlations between Al and Sc, Zr and Th (R^2 = 0.63, 0.64 and 0.50 respectively, n = 53; Fig. 6), indicating that the Al originates from a common siliciclastic flux. The black shale sample ZN04-55 plots far away from the Al–Sc regression

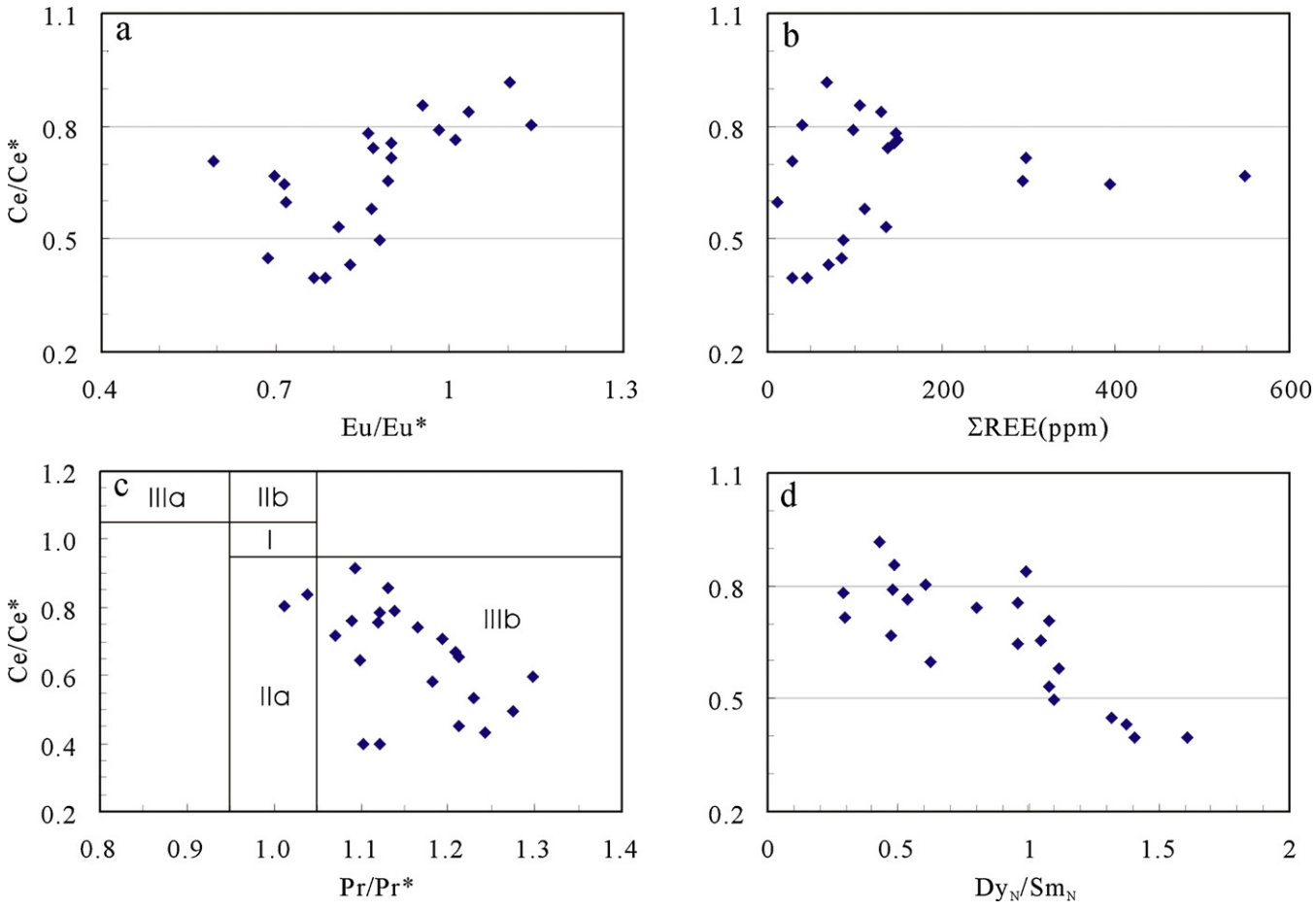

Fig. 4. Plots of Ce anomalies to (a) Eu anomalies, (b) bulk REE, (c) Pr anomalies, and (d) Dy_N/Sm_N ratios calculated from the PAAS shale-normalized REE abundances of organic matter in sedimentary rocks from the Zhongnancun section in Zunyi, South China. Field I, no anomaly; Field IIa, positive La anomaly causes apparent negative Ce anomaly; Field IIb, negative La anomaly causes apparent positive Ce anomaly; Field IIIa, real positive Ce anomaly; Field IIIb, real negative Ce anomaly.

line but around the other two regression lines (Fig. 6). This may result from an input of external Sc. The Ni–Mo sulphide ore, V ore, phosphatic concretion and cherts plot on or around those regression lines (Fig. 6), indicating that their detrital sources are similar to the black shales. The three tuffs (ZN04-21, ZN04-22 and ZN04-23-2) are aligned along other regression lines (R^2 = 0.88, 1.00 and 0.89, respectively; Fig. 6). They represent an Al-rich source, which may explain their lower metal/Al ratios. In general, we feel justified in using the Al-normalized procedure in our samples, except for the three tuffs, to look for trace element enrichments beyond the detrital flux.

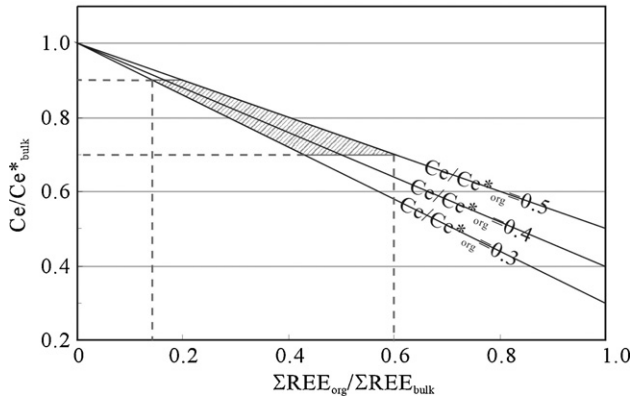

Fig. 5. Illustration of Ce anomalies in bulk rocks varying with REE contributions and Ce anomalies of organic matter. Negative Ce anomalies from 0.7 to 0.9 in bulk rocks correspond to 15–60% of bulk REE contributed by organic matter with Ce/Ce^* = 0.3–0.5.

The use of enrichment factors (relative to certain shale standards, such as the PAAS or Black Sea euxinic sediments) of trace elements and their relationships to TOC to trace paleoredox conditions has been boldly extended from modern sediments to ancient shales (e.g., Kimura and Watanabe, 2001; Lyons et al., 2003; Algeo and Maynard, 2004; Naimo et al., 2005). According to those studies, the trace elements U, V and Mo show potential for discerning redox conditions (Algeo and Lyons, 2006; Tribovillard et al., 2006; Zhou and Jiang, 2009). In the following subsections, we will use these proxies to explore early Cambrian environments.

Uranium is present mainly in the soluble form of uranyl carbonate complexes [$UO_2(CO_3)_3^{4-}$] in oxic to suboxic marine settings, but it can be reduced to U(IV) and precipitates into the sediments as crystalline uraninite (UO_2) or its metastable precursors under certain reducing conditions (Anderson et al., 1989; Calvert and Pedersen, 1993). Since the reduction of U(VI) to U(IV) is most probably mediated by bacterial sulphate reduction and the intensity of sulphate reduction activity is linked to the abundance of organic matter, U concentrations usually show a good correlation with TOC concentrations in non-sulphidic anoxic facies (Tribovillard et al., 2006 and references therein). In sulphidic euxinic facies, the U concentrations increase substantially, but the U–TOC correlation becomes weak or disappears (Tribovillard et al., 2006). In the present study, the U/Al ratios (ppm/%) in the black shales vary between 1.48 and 34.1, which are at least five times higher than

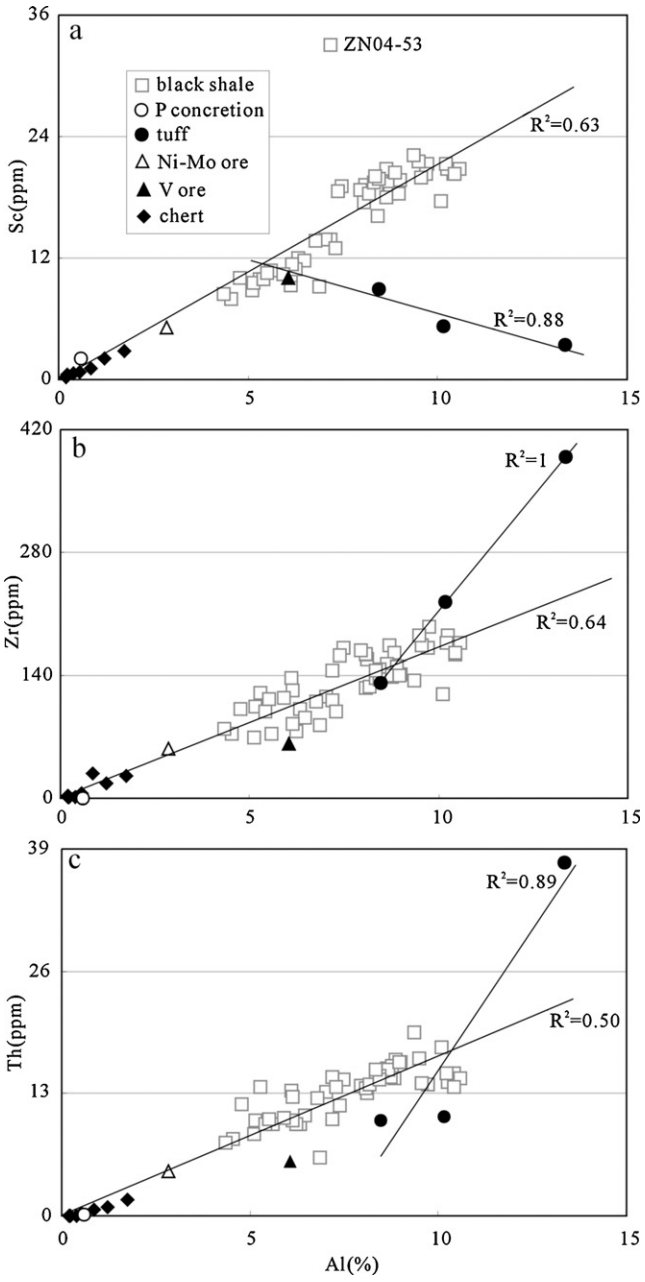

Fig. 6. Correlations between Al and Sc, Zr, Th for samples in the Zhongnancun section in Zunyi, South China. Note that black shales, cherts, Ni–Mo sulphide ore and V ore can be fitted by good regression lines, indicating their common source region for the detrital fractions; while the tuffs form a different regression line.

in the PAAS shale standard (0.31; Taylor and McLennan, 1985). When compared to the Black Sea sulphidic (euxinic) sediment, where the U/Al ratio is 3.3 (Calvert and Pedersen, 1993), the lower black shales exhibit relative U enrichments, while most upper black shales exhibit variable U depletions (Fig. 2b). Generally, this could be taken to indicate that the lower black shales were deposited under sulphidic conditions similar to the Black Sea, and the upper black shales were deposited under relatively less reducing conditions (e.g., Guo et al., 2007a; Zhou and Jiang, 2009). However, the U/Al ratios in our black shale samples correlate well with the TOC abundances (R^2 = 0.77, n = 52 without sample ZN04-55; Fig. 7a), indicating that redox conditions were generally anoxic but not sulphidic (e.g., Algeo and Maynard, 2004). Because trace element–TOC correlations seem more effective in discerning redox grade (Tribovillard et al., 2006), we consider that redox conditions may have been less reducing than might otherwise be presumed from the high U/Al ratios.

Vanadium is preferentially concentrated in reducing sediments relative to oxic sediments (Tribovillard et al., 2006). The removal of V from the water column to sediments relates to two reduction reactions. One is the reduction of V(V) to V(IV), which occurs under non-sulphidic anoxic conditions and is facilitated by humic and fulvic acids. In this case, V abundances usually correlate well with TOC abundances (Morford and Emerson, 1999). The other is the reduction of V(IV) to V(III), which takes place under sulphidic conditions (Morford and Emerson, 1999). In this case, V abundances display no obvious correlation with TOC abundances. In the present study, the V/Al ratios (ppm/%) in the black shales vary between 24.9 and 1403, which are far higher than that in the PAAS shale standard (15.0; Taylor and McLennan, 1985). Unlike with U, almost all the black shale samples (except two) display V enrichments compared to Black Sea sediment (V/Al = 28.8; Calvert and Pedersen, 1993), and there is no clear correlation between V/Al ratios and TOC abundances (R^2 = 0.35, n = 53; Fig. 7b). This situation points to sulphidic conditions during black shale deposition. However, the upper part black shales display good V/Al–TOC correlation (R^2 = 0.71, n = 27; Fig. 7b). This supports the case for non-sulphidic but anoxic conditions during deposition of the upper part black shales.

Molybdenum is a conservative element in the oxic marine environment (Algeo and Lyons, 2006). Its removal from the water column to sediments requires a reduction reaction through which H_2S/HS^- transforms stable molybdate to particle-reactive thiomolybdates (Helz et al., 1996). Since the H_2S/HS^- is largely produced from the interaction between organic matter and sulphate reducing bacteria, authigenic Mo accumulations are closely related to organic matter. This relation is evinced by the positive correlation between Mo and TOC concentration in non-sulphidic anoxic sediments (Tribovillard et al., 2006). Under sulphidic conditions, the presence of free H_2S leads to further Mo enrichment which breaks the Mo–TOC correlation. In the present study, the Mo/Al ratios (ppm/%) in the black shales vary between 0.32 and 69.2, which is far higher than with the PAAS shale standard (0.10; Taylor and McLennan, 1985). As with the U/Al ratios, Mo displays enrichments in the lower black shales and depletions in the upper black shales compared to Black Sea sulphidic sediment (4.3; Calvert and Pedersen, 1993), and exhibits a positive correlation with TOC contents (R^2 = 0.64, n = 50 without three samples: ZN04-50, ZN04-59 and ZN04-71; Fig. 7c). This indicates that Mo enrichment by the black shales occurred under generally non-sulphidic anoxic conditions.

From the discussions above, it can be seen that: (1) all the black shales display concurrent U, V, and Mo enrichments relative to the PAAS shale standard, (2) only the lower black shales display concurrent U, V and Mo enrichment compared to Black Sea sediment, and (3) the upper black shales show good metal–TOC correlations. From these features, we can conclude that the redox conditions of the local sedimentary environment were generally sulphidic in the lower black shales and changed to non-sulphidic anoxic in the upper black shales.

5.3. Origin of the polymetallic Ni–Mo sulphide ore

The origin of the polymetallic Ni–Mo sulphide ore has been debated for many years (e.g., Fan et al., 1984; Coveney et al., 1992; Murowchick et al., 1994; Lott et al., 1999; Jiang et al., 2004; Steiner et al., 2001; Mao et al., 2002; Pan et al., 2004; Yang et al., 2004; Jiang et al., 2006, 2007a,b, 2008, 2009; Lehmann et al., 2007; Orberger et al., 2007). The key problem is the source of the metals. Mao et al. (2002) and Lehmann et al. (2007) presumed that the metals derived from ambient seawater, while Jiang et al. (2004, 2006, 2007a,b) and

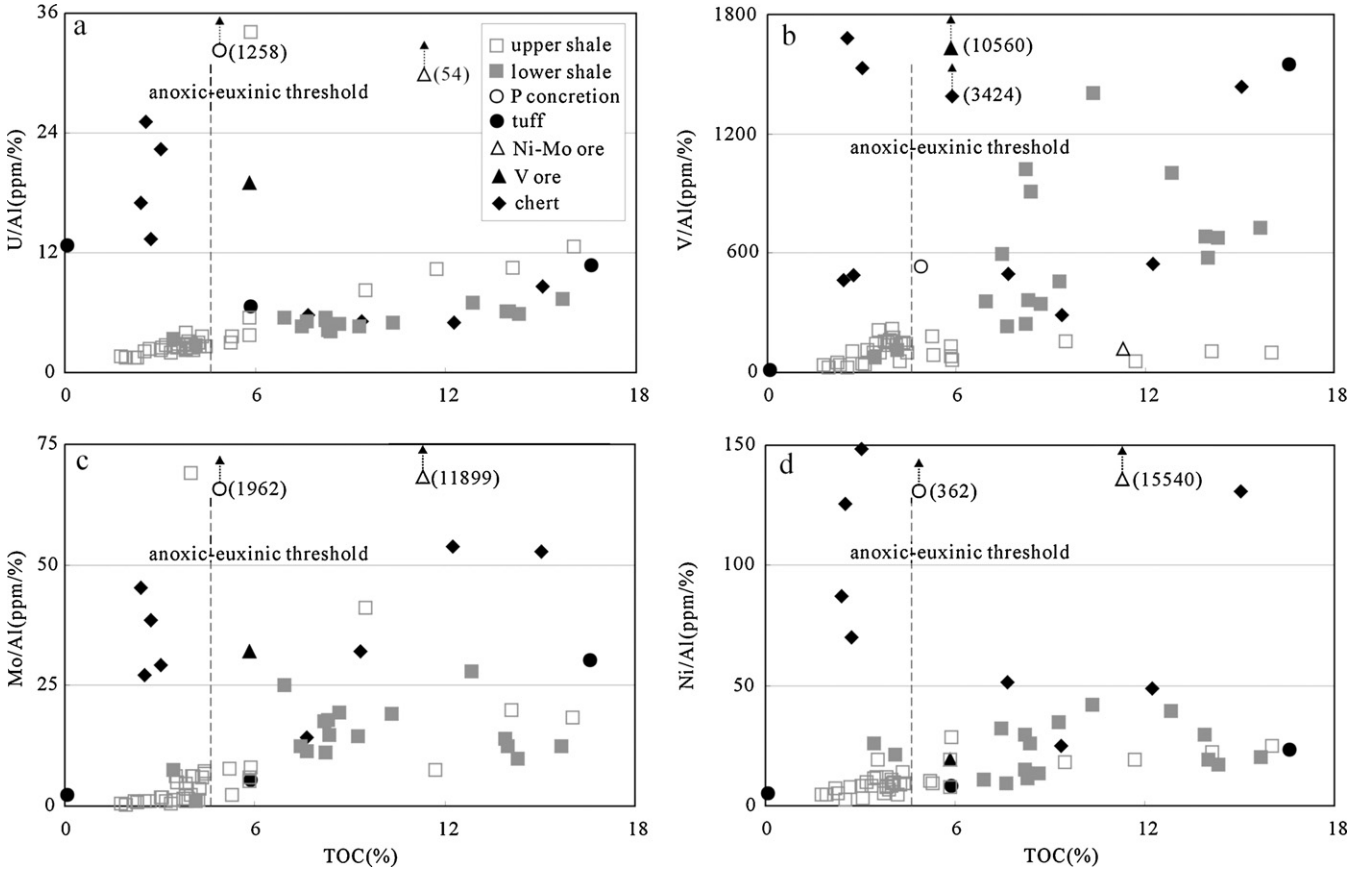

Fig. 7. Correlations between TOC with (a) U/Al, (b) V/Al, (c) Mo/Al, and (d) Ni/Al for samples from the Zhongnancun section in Zunyi, South China. Good correlations are observed when TOC abundances are below 4.5%, where anoxic depositional conditions are suggested. In addition, the Ni–Mo sulphide ore plot out of the fields, indicating a hydrothermal origin of those trace elements.

others (e.g., Lott et al., 1999; Steiner et al., 2001; Pan et al., 2004; Yang et al., 2004) ascribed their enrichment to hydrothermal venting. An alternative model has been proposed by Emsbo et al. (2005) who suggested the discharge of petroleum together with diverse hydrothermal fluids into the basin. Although a full discussion on the origin of the metal enrichments is not the purpose of the present study, our trace element and TOC data contributes to resolving this problem.

Firstly, the polymetallic Ni–Mo sulphide ore has Mo/TOC ratios up to 3000. Over geological time periods, the Mo/TOC ratios in normal euxinic sediments do not rise over 100 and remain mostly below 50 (Scott et al., 2008). Our Mo/TOC ratio for the polymetallic Ni–Mo ore layer is at least 30 times greater than the upper limit value, indicating that an additional source supplied Mo, and we consider the hydrothermal venting was a likely source.

Secondly, the polymetallic Ni–Mo sulphide ore has a Ni/TOC ratio up to 3912, which is far greater than that of normal black shales (<100). Ni is a typical micronutrient element (Calvert and Pedersen, 1993; Algeo and Maynard, 2004). Its removal from the water column to sediments mainly depends on biotic processes (Nameroff et al., 2004; Piper and Perkins, 2004; Naimo et al., 2005). The extremely high Ni/TOC ratio, thus, requires an additional mechanism of enrichment other than normal biotic accumulation. Remobilization from overlying strata with higher TOC contents could be a possibility, but the lack of gradient in Ni content from the polymetallic Ni–Mo ore to upper strata samples argues against this possibility. An alternative is that hydrothermal vents effused Ni into sulphidic bottom waters so forming NiS precipitate directly.

Thirdly, the polymetallic Ni–Mo sulphide ore has a U/TOC ratio of up to 14. This relatively high value also requires input of external U. According to these geochemical arguments, we suggest that the polymetallic Ni–Mo sulphide ore is linked to hydrothermal vents, which provided some amount of Ni, Mo and U into sulphidic bottom waters. After combining with H_2S, those metals formed sulphides and precipitated into sediments.

6. Conclusions

1. REE of kerogen in early Cambrian Niutitang black shales from Zunyi, South China displays a PAAS shale-normalized pattern unlike those of modern seawater, but with evident negative Ce anomalies, reflecting the oxic environment of surface productivity rather than the more reducing environment of bottom waters. Mass balance calculation indicates that the extent of the negative Ce anomaly in bulk black shales depends on the REE contribution from organic matter and its primary Ce/Ce^* value.
2. Trace element contents of U, V, and Mo in early Cambrian Niutitang black shales from Zunyi, South China reveal that the bottom waters were sulphidic (euxinic) in the lower part and changed to non-sulphidic anoxic in the upper part. The presence of sponge spicules indicates that they rapidly colonized the benthic environment when it became less reducing.
3. The geochemical behavior of U, Ni and Mo in the ocean and their super-enrichments in the polymetallic Ni–Mo sulphide ore layer supports the link of the extreme metal enrichments to hydrothermal vents which supplied a significant amount of metals to the sulphidic bottom waters, where they combined with H_2S to form sulphides and then precipitated into sediments.

Acknowledgements

We wish to sincerely thank Hai-Ling Deng, Qing-Jun Guo, Kui-Dong Zhao, Wei-Guang Zhu, Chao-Yang Li and Yu-Ping Liu for their assistance in the field and valuable discussion. Yi Hu from the Advanced Analytical Centre in James Cook University, Australia helped the laboratory work. This research is supported by National Science Foundation of China (40872026, 40803013), Key Project of Chinese Ministry of Education (306007), and CAS Dean Honor Special Fund (No. 35-20).

References

Algeo, T.J., Lyons, T.W., 2006. Mo–total organic carbon covariation in modern anoxic marine environments: implications for analysis of paleoredox and paleohydrographic conditions. Paleoceanography 21, PA1016.

Algeo, T.J., Maynard, J.B., 2004. Trace-element behavior and redox facies in core shales of Upper Pennsylvanian Kansas-type cyclothems. Chemical Geology 206, 289–318.

Amthor, J.E., Grotzinger, J.P., Schröder, S., Bowring, S.A., Ramezani, J., Martin, M.W., Matter, A., 2003. Extinction of *Cloudina* and *Namacalathus* at the Precambrian–Cambrian boundary in Oman. Geology 31 (5), 431–434.

Anderson, R.F., Fleisher, M.Q., LeHuray, A.P., 1989. Concentration, oxidation state and particulate flux of uranium in the Black Sea. Geochimica et Cosmochimica Acta 53, 2205–2213.

Brasier, M., 1992. Background to the Cambrian explosion. Journal of Geological Society London 149, 585–587.

Brasier, M.D., Magaritz, M., Corfield, R., Luo, H., Wu, X., Ouyang, L., Jiang, Z., Hamadi, B., He, T., Frazier, A.G., 1990. The carbon- and oxygen-isotopic record of the Precambrian–Cambrian boundary interval in China and Iran and their corre1ation. Geological Magazine 127, 319–332.

Calvert, S.E., Pedersen, T.F., 1993. Geochemistry of recent oxic and anoxic marine sediments: implications for the geological record. Marine Geology 113, 67–88.

Coveney Jr., R.M., Murowchick, J.B., Grauch, R.I., Michael, D., Glascock, D., Denison, J.D., 1992. Gold and platinum in shales with evidence against extraterrestrial sources of metals. Chemical Geology 99, 101–114.

Coveney Jr., R.M., 2003. Re–Os dating of polymetallic Ni–Mo–PGE–Au mineralization in lower Cambrian black shales of South China and its geologic significance: a discussion. Economic Geology 98, 661–665.

Elderfield, H., Greaves, M.J., 1982. The rare earth elements in seawater. Nature 296, 214–219.

Emsbo, P., Hofstra, A., Johnson, C.A., Koenig, A., Grauch, R., 2005. Lower Cambrian metallogenesis of south China: Interplay between diverse basinal hydrothermal fluids and marine chemistry. In: Mao, J., Bierlein, F.P. (Eds.), 8th Biennial SGA Meeting, Mineral Deposit Research: Meeting the Global Challenge, 1. Springer, Beijing, pp. 115–118.

Fan, D., 1983. Polyelements in the Lower Cambrian black shale series in southern China. In: Augustithis, S.S. (Ed.), The Significance of Trace Metals in Solving Petrogenetic Problems and Controversies. Theophrastus, Athens, pp. 447–474.

Fan, D., Yang, R., Huang, Z., 1984. The Lower Cambrian black shales series and the iridium anomaly in south China , Academia Sinica, Developments in Geoscience, Contributions to the 27th IGC, Moscow. Science Press, Beijing, pp. 215–224.

Felitsyn, S., Morad, S., 2002. REE patterns in latest Neoproterozoic-early Cambrian phosphate concretions and associated organic matter. Chemical Geology 187, 257–265.

Felitsyn, S.B., Vidal, G., Moczydlowska, M., 1998. Trace elements and Sr and C isotopic signatures in late Neoproterozoic and earliest Cambrian sedimentary organic matter from siliciclastic successions in the East European Platform. Geological Magazine 135, 537–551.

Feng, H.Z., Ling, H.F., Jiang, S.Y., Yang, J.H., 2004. $\delta^{13}C_{car}$ and Ce_{anom} excursions in the post-glacial neoproterozoic and early Cambrian interval in Guizhou, South China. Progress in Natural Science (Special issue), 154–158.

German, C.R., Elderfield, H., 1990. Application of the Ce anomaly as paleoredox indicator: the ground rules. Paleooceanography 5, 823–833.

Goldberg, T., Strauss, H., Guo, Q., Liu, C., 2007. Reconstructing marine redox conditions for the early Cambrian Yangtze Platform: Evidence form biogenic sulphur and organic carbon isotopes. Palaeogeography, Palaeoclimatology, Palaeoecology 254, 175–193.

Guo, Q., Shields, G.A., Liu, C., Strauss, H., Zhu, M., Pi, D., Goldberg, T., Yang, X., 2007a. Trace element chemostratigraphy of two Ediacaran–Cambrian successions in South China: implications for organosedimentary metal enrichment and silicification in the early Cambrian. Palaeogeography, Palaeoclimatology, Palaeoecology 254, 194–216.

Guo, Q., Strauss, H., Liu, C., Goldberg, T., Zhu, M., Pi, D., Heubeck, C., Vernhet, E., Yang, X., Fu, P., 2007b. Carbon isotopic evolution of the terminal neoproterozoic and early Cambrian: evidence from the Yangtze platform, South China. Palaeogeography, Palaeoclimatology, Palaeoecology 254, 140–157.

Helz, G.R., Miller, C.V., Charnock, J.M., Mosselmans, J.F.W., Pattrick, R.A.D., Gamer, C.D., Vaughan, D.J., 1996. Mechanism of molybdenum removal from the sea and its concentration in black shales: EXAFS evidence. Geochimica et Cosmochimica Acta 60, 3631–3642.

Horan, M.F., et al., 1994. Rhenium and osmium isotopes in black shales and Ni–Mo–PGE rich sulfide layers, Yukon Territory, Canada, and Hunan and Guizhou Provinces, China. Geochimica Cosmochimica Acta 58, 257–261.

Jiang, S.Y., Yang, J.H., Ling, H.F., Feng, H.Z., Chen, Y.Q., Chen, J., 2004. Re–Os isotopes and PGE geochemistry of black shales and intercalated Ni–Mo polymetallic sulfide bed from the Lower Cambrian Niutitang Formation, South China. Progress in Natural Science (Special issue), 18–24.

Jiang, S.Y., Chen, Y.Q., Ling, H.F., Yang, J.H., Feng, H.Z., Ni, P., 2006. Trace- and rare-earth element geochemistry and Pb–Pb dating of black shales and intercalated Ni–Mo–PGE–Au sulfide ores in Lower Cambrian strata, Yangtze Platform, South China. Mineralium Deposita 41 (5), 453–467.

Jiang, S.Y., Yang, J.H., Ling, H.F., Chen, Y.Q., Feng, H.Z., Zhao, K.D., Ni, P., 2007a. Extreme enrichment of polymetallic Ni–Mo–PGE–Au in lower Cambrian black shales of South China: An Os isotope and PGE geochemical investigation. Palaeogeography, Palaeoclimatology, Palaeoecology 254, 217–228.

Jiang, S.Y., Zhao, H.X., Chen, Y.Q., Yang, T., Yang, J.H., Ling, H.F., 2007b. Trace and rare earth element geochemistry of phosphate nodules from the lower Cambrian black shale sequence in the Mufu Mountain of Nanjing, Jiangsu province, China. Chemical Geology 244, 584–604.

Jiang, S.Y., Zhao, K.D., Li, L., Ling, H.F., Zhu, M., 2008. Highly metalliferous carbonaceous shale and Early Cambrian seawater: comment. Geology, e158–e159.

Jiang, S.Y., Pi, D.H., Heubeck, C., Frimmel, H., Liu, Y.P., Deng, H.L., Ling, H.F., Yang, J.H., 2009. Early Cambrian ocean anoxia in South China. Nature 459, e5–e6.

Kimura, H., Watanabe, Y., 2001. Oceanic anoxia at the Precambrian–Cambrian boundary. Geology 29, 995–998.

Kříbek, B., Sýkorová, I., Pašava, J., Machovič, V., 2007. Organic geochemistry and petrology of barren and Mo–Ni–PGE mineralized marine black shales of the lower Cambrian Niutitang formation (South China). International Journal of Coal Geology 72, 240–256.

Kryc, K.A., Murray, R.W., Murray, D.W., 2003. Al-to-oxide and Ti-to-organic linkage in biogenic sediments: relationship to paleoexport production and bulk Al/Ti. Earth Planetary Science Letter 211, 125–141.

Lehmann, B., Nägler, T.F., Holland, H.D., Wille, M., Mao, J., Pan, J., Dulski, P., 2007. Highly metalliferous carbonaceous shale and early Cambrian seawater. Geology 35, 403–406.

Lewan, M.D., 1986. Stable carbon isotopes of amorphous kerogens from Phanerozoic sedimentary rocks. Geochimica et Cosmochimica Acta 50, 1583–1591.

Li, S., Xiao, Q., Shen, J., Sun, L., Liu, B., Yang, B., Jiang, Y., 2003. Rhenium–osmium isotope constraints on the age and source of the platinum mineralization in the lower Cambrian black rock series of Hunan–Guizhou provinces, China. Science in China Series D: Earth Sciences 46, 919–927.

Li, G., Steiner, M., Zhu, X., Yang, A., Wang, H., Erdtmann, B.D., 2007. Early Cambrian metazoan fossil record of South China: Generic diversity and radiation patterns. Palaeogeography, Palaeoclimatology, Palaeoecology 254, 229–249.

Lott, D.A., Coveney Jr., R.M., Murowchick, J.B., 1999. Sedimentary exhalative nickel–molybdenum ores in south China. Economic Geology 94, 1051–1066.

Lyons, T.W., Werne, J.P., Hollander, D.J., Murray, R.W., 2003. Contrasting sulfur geochemistry and Fe/Al and Mo/Al ratios across the last oxic-to anoxic transition in the Cariaco Basin, Venezuela. Chemical Geology 195, 131–157.

Mao, J., Lehmann, B., Du, A., Zhang, G., Ma, D., Wang, Y., Zeng, M., Kerrich, R., 2002. Re–Os dating of polymetallic Ni–Mo–PGE–Au mineralization in Lower Cambrian black shales of South China and its geologic significance. Economic Geology 97, 1051–1061.

McKerrow, W.S., Scotese, C.R., Brasier, M.D., 1992. Early Cambrian continental reconstructions. Journal of the Geological Society 149, 599–606.

McLennan, S.M., 1989. Rare earth elements in sedimentary rocks: influence of provenance and sedimentary processes. In: Lipin, B.R., Mckay, G.A. (Eds.), Geochemistry and Mineralogy of Rare Earth Elements. Reviews in Mineralogy and Geochemistry, vol. 21, pp. 169–200.

Morford, J.L., Emerson, S., 1999. The geochemistry of redox sensitive trace metals in sediments. Geochimica et Cosmochimica Acta 63, 1735–1750.

Mossman, D.J., Goodarzi, F., Gentzis, T., 1993. Characterization of insoluble organic matter from the Lower Proterozoic Huronian Supergroup, Elliot Lake. Precambrian Research 61, 279–293.

Murowchick, J.B., Coveney Jr., R.M., Grauch, R.I., Eldridge, C.S., Shelton, K.L., 1994. Cyclic variations of sulfur isotopes in Cambrian Stratabound Ni–Mo–(PGE–Au) ores of southern China. Geochimica et Cosmochimica Acta 58, 1813–1823.

Naimo, D., Adamo, P., Imperato, M., Stanzione, D., 2005. Mineralogy and geochemistry of a marine sequence, Gulf of Salerno, Italy. Quaternary International 140–141, 53–63.

Nameroff, T.J., Calvert, S.E., Murray, J.W., 2004. Glacial–interglacial variability in the eastern tropical North Pacific oxygen minimum zone recorded by redox-sensitive trace metals. Paleoceanography 19, PA1010.

Orberger, B., Vymazalova, A., Wagner, C., Fialin, M., Gallien, J.P., Wirth, R., Pasava, J., Montagnac, G., 2007. Biogenic origin of intergrown Mo–sulphide- and carbonaceous matter in lower Cambrian black shales (Zunyi Formation, southern China). Chemical Geology 238, 213–231.

Pan, J., Ma, D., Cao, S., 2004. Trace element geochemistry of the lower Cambrian black rock series from northwestern Hunan, South China. Progress in Natural Science (Special issue), 64–70.

Piper, D.Z., Perkins, R.B., 2004. A modern vs. Permian black shale – the hydrography, primary productivity, and water-column chemistry of deposition. Chemical Geology 206, 177–197.

Sawaki, Y., Nishizawa, M., Suo, T., Komiya, T., Hirata, T., Takahata, N., Sano, Y., Han, J., Kon, Y., Maruyama, S., 2008. Internal structures and U–Pb ages of zircons

from a tuff layer in the Meishucunian formation, Yunnan Province, South China. Gondwana Research 14 (1–2), 148–158.
Scott, C., Lyons, T.W., Bekker, A., Shen, Y., Poulton, S.W., Chu, X., Anbar, A.D., 2008. Tracing the stepwise oxygenation of the Proterozoic ocean. Nature 452, 456–459.
Shen, Y., Schidlowski, M., 2000. New C isotope stratigraphy from southwest China: implications for the placement of the Precambrian–Cambrian boundary on the Yangtze Platform and global correlations. Geology 28, 623–626.
Shen, Y., Schidlowski, M., Chu, X., 2000. Biogeochemical approach to understanding phosphogenic events of the terminal Proterozoic to Cambrian. Palaeogeography, Palaeoclimatology, Palaeoecology 158, 99–108.
Shen, Y., Zhao, R., Chu, X., Lei, J., 1998. The carbon and sulfur isotope signatures in the Precambrian–Cambrian transition series of the Yangtze Platform. Precambrian Research 89, 77–86.
Shields, G., Stille, P., 2001. Diagenetic constrains on the use of cerium anomalies as palaeoseawater proxies: an isotopic and REE study of Cambrian phosphorites. Chemical Geology 175, 29–48.
Shields, G.A., Webb, G.E., 2004. Has the REE composition of seawater changed over geological time? Chemical Geology 204, 103–107.
Sholkovitz, E., Landing, W.M., Lewis, B.L., 1994. Ocean particle chemistry: the fractionation of the rare earth elements between suspended particles and seawater. Geochimica et Cosmochimica Acta 58, 1567–1580.
Steiner, M., Li, G., Qian, Y., Zhu, M., Erdtmann, B.-D., 2007. Neoproterozoic to Early Cambrian small shelly fossil assemblages and a revised biostratigraphic correlation of the Yangtze Platform (China). Palaeogeography, Palaeoclimatology, Palaeoecology 254, 67–99.
Steiner, M., Willis, E., Erdtmann, B.D., Zhao, Y.L., Yang, R.D., 2001. Submarine-hydrothermal exhalative ore layers in black shales from South China and associated fossils: insights into a Lower Cambrian facies and bio-evolution. Palaeogeography, Palaeoclimatology, Palaeoecology 169, 165–191.
Taylor, S.R., McLennan, S.M., 1985. The Continental Crust: Its Composition and Evolution. Blackwell, Oxford, pp. 46–92.
Tribovillard, N., Algeo, T.J., Lyons, T., Riboulleau, A., 2006. Trace metals as paleoredox and paleoproductivity proxies: an update. Chemical Geology 232, 12–32.
Weber, B., Steiner, M., Zhu, M., 2007. Precambrian–Cambrian trace fossils from the Yangtze Platform (South China) and the early evolution of bilaterian lifestyles. Palaeogeography, Palaeoclimatology, Palaeoecology 254, 328–349.
Wille, M., Nägler, T.F., Lehmann, B., Schröder, S., Kramers, J.D., 2008. Hydrogen sulphide release to surface waters at the Precambrian/Cambrian boundary. Nature 453, 767–769.
Wright, J., Schrader, H., Holser, W.T., 1987. Paleoredox variations in ancient oceans recorded by rare earth elements in fossil apatite. Geochimica et Cosmochimica Acta 51, 631–644.
Yang, J.H., Jiang, S.Y., Ling, H.F., Feng, H.Z., Chen, Y.Q., Chen, J., 2004. Paleoceangraphic significance of redox-sensitive metals of black shales in the basal Lower Cambrian Niutitang Formation in Guizhou Province, South China. Progress in Natural Science (Special issue), 118–123.
Yang, Z.W., 2008. The basic feature and origin of the black shale type vanadium deposit in eastern Guizhou: taking the Jianggu Vanadium deposit in Zhenyuan County as an example. Guizhou Geology 25, 31–34.
Zhang, A.Y., Wu, D.M., Guo, L., Wang, Y.L., 1987. The Geochemistry of Marine Black Shale Formation and its Metallogenic Significance. Science Publishing House, p. 225.
Zhou, C.M., Jiang, S.Y., 2009. Palaeoceanographic redox environments for the lower Cambrian Hetang Formation in South China: Evidence from pyrite framboids, redox-sensitive trace elements, and sponge biota occurrence. Palaeogeography, Palaeoclimatology, Palaeoecology 271, 279–286.
Zhu, M., Zhang, J., Steiner, M., Yang, A., Li, G., Erdtmann, B.D., 2004. Sinian–Cambrian stratigraphic framework for shallow- to deep-water environments of the Yangtze Platform: an integrated approach. Progress in Natural Science (Special issue), 75–84.
Zhu, R.X., Li, X.H., Hou, X.G., Pan, Y.X., Wang, F., Deng, C.L., He, H.Y., 2009. SIMS U–Pb zircon age of a tuff layer in the Meishucun section, Yunnan, southwest China: constraint on the age of the Precambrian–Cambrian boundary. Science in China Series D-Earth Sciences 52, 1385–1392.